# On the generation of chatter marks in peripheral milling: A spectral interpretation

# Accepted Manuscript


On the generation of chatter marks in peripheral milling: A spectral interpretation

N. Grossi, A. Scippa, L. Sallese, F. Montevecchi, G. Campatelli

PII: S0890-6955(18)30120-2

DOI: 10.1016/j.ijmachtools.2018.05.008

Reference: MTM 3353

To appear in: *International Journal of Machine Tools and Manufacture*

Received Date: 8 February 2018

Revised Date: 29 May 2018

Accepted Date: 31 May 2018

Please cite this article as: N. Grossi, A. Scippa, L. Sallese, F. Montevecchi, G. Campatelli, On the generation of chatter marks in peripheral milling: A spectral interpretation, *International Journal of Machine Tools and Manufacture* (2018), doi: 10.1016/j.ijmachtools.2018.05.008.

**On the generation of chatter marks in peripheral milling: a spectral interpretation**

N. Grossi[a,*], A. Scippa[a], L. Sallese[a], F. Montevecchi[a], G. Campatelli[a]

[a]Department of Industrial Engineering, University of Firenze, via di Santa Marta 3, 50139, Firenze, Italy.

*corresponding author. Tel. +39 055 2758726. E-mail: niccolo.grossi@unifi.it

**Title**

On the generation of chatter marks in peripheral milling: a spectral interpretation

**Abstract**

Chatter vibration induces a characteristic pattern on the milled surface, known as chatter marks, causing a poor surface quality. While several works deal with the prediction of the machined surface in stable condition, surface under chatter vibration has not been extensively studied: it is not clear how vibrations at high chatter frequency return highly spaced chatter marks on the surface. This paper investigates the chatter marks generation mechanisms focusing on this issue, i.e., on the surface spectral proprieties. The generation of the surface profile is regarded as a problem of sampling at the tooth pass frequency (in the time domain) and reconstruction (in the spatial domain) of the cutting tool displacements. Using this analogy, the paper highlights two main effects (aliasing and pseudo moiré), proposing specific formulations. The method is validated by a numerical investigation, based on a surface generation model coupled with a time-domain simulator of the milling process. Finally, an experimental validation is proposed. The formulations presented in this work provide an insight in the relation between chatter frequency and chatter marks pattern. Therefore, if the chatter frequency pattern over the spindle speed is known (e.g., identified via simulations or experiments), the proposed method could support the selection of cutting parameters which results in an acceptable surface, even in highly unstable cutting conditions.

*Keywords*: Chatter; Dynamics; Milling; Surface analysis; Chatter marks.

## 1. INTRODUCTION

Surface quality and roughness of milled products are key features to assess the process performances. Achieving the optimal tradeoff between the maximization of productivity and the surface topography tolerances is a challenging task of modern milling process [1], which requires a deep investigation on machined surface characteristics to support cutting parameters selection. In the last decades, both process modeling approaches [2] and experimental methods [3][4] were proposed, with the aim of studying different effects on the surface (e.g., tool run-out [5], tool deflection [6] and form errors [7]). Among them, vibrations are one of the most critical, since the analysis of the surface altered by these phenomena requires the study of several factors, such as machine tool dynamics, cutting forces and surface generation mechanism [2].

Two are the main types of vibrations affecting the milling process: i) forced vibration, induced by the periodic nature of the process that excites the tool and the workpiece at the tooth pass frequency and its harmonics; ii) self-excited chatter vibration, occurring at specific cutting conditions and characterized by a regenerative behavior, which produces poor surface quality with a specific surface pattern, known as chatter marks.

On one hand, several models aiming at predicting the milled surface topography under the effect of forced vibrations have been presented. Schmitz et al. [2] proposed closed formulation to estimate the milled surface error and more recently investigate the effect of run-out on the surface [5]. These models are generally focused on the form errors, known as Surface Location Error (SLE), without investigating the surface at the roughness level in the spatial frequency domain, that would imply a very high computational cost, since several points on the surface are required.

On the other hand, for what concern self-excited vibration, very few works have been proposed on the analysis of chatter marks pattern in milling.

This paper provides an insight on the milled surface generation mechanism, analyzing the surface spatial frequency content in relation to the characteristic frequency of the phenomena and focusing on chatter vibration (i.e., chatter frequency) and chatter marks pattern.

Indeed, although chatter should be predicted and avoided [8], when chatter-free strategy cannot be pursued since they cause an unacceptable reduction of productivity, forecasting the milled surface could be useful to select cutting parameters which mitigate the chatter detrimental effect, resulting in the desired chatter marks pattern. Moreover, since the regenerative nature of chatter depends on

the surface altered by vibrations, investigating the surface generation mechanism could support the study of corrective measure to predict/suppress this detrimental phenomenon.
Some studies on chatter effects on the surface for different machining operations, such as turning [9] or grinding [10] were presented. In turning, Lin and Chang [11] investigated the machined surface affected by vibrations through a dedicated model, finding out that the vibrations on radial direction and the vibration frequency/rotational speed ratio are key factors. Plaza et al.[12] experimentally analyzed the turned surface affected by chatter, focusing on the roughness values, while Moon and Sutherland [9] investigated the machined surface in the spatial frequency domain, highlighting its dependency on the relation between rotation and vibration frequency.
In milling, Seguy et al. proposed a method to simulate machined surface of thin-walls [13], while Peigné et al. [14] focused their work on surface roughness in small radial immersion milling. Recently, Shiota et al. [15] proposed a theory on chatter marks distribution. However, the presented experimental result showed some discrepancies, suggesting the presence of additional effects on the surface pattern. Lei and Soshi [16] developed a method to optimize the milling process parameters on the basis of chatter marks distribution acquired by a dedicated vision system. Stepan et al.[17] proposed the adoption of two-dimensional Fourier transform (2DFFT) to analyze the milled surface with the aim of distinguishing between stable and unstable cutting. However, the chatter marks pattern and spatial frequencies were not deeply investigated, leaving unanswered the following question: "How tool vibrations at high chatter frequency produce low frequency marks (i.e., wide marks) on the surface?".
This paper addresses this issue, proposing a new approach to describe the milled surface under vibrations effects. The generation of the surface profile is regarded as a problem of sampling at the surface generation frequency (i.e., tooth pass frequency) of the cutting tool displacements (i.e., vibrations). The chatter marks pattern is hence described considering the sampling theorem and the effects of under sampling. Analytical formulations to compute surface spectral proprieties are proposed, requiring few inputs (tooth pass frequency, feed per tooth and chatter frequency) to return the chatter marks distribution, without requiring time-consuming and demanding approaches, involving the model of the whole milling process. A milled surface generation model is combined with a time-domain simulator of the milling process to validate the proposed approach on several numerical configurations and conditions. Finally, an experimental validation is provided to show the accuracy of the proposed formulations.

## 2. CHATTER MARKS GENERATION

The machined surface profile is the envelope of all the traces of the cutter's edges with respect to the workpiece. As shown in Fig. 1a, in the kinematic case (i.e., without vibrations), when the tool trajectory is defined by the nominal feed only, the trochoidal path of the cutting edges produces a series of regular arc segments, the feed marks.

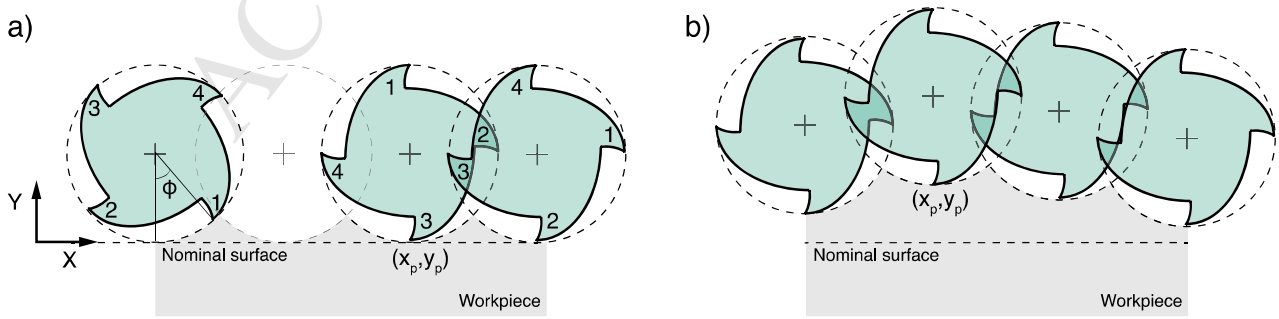


*Fig. 1 Milled surface: a) kinematic (i.e., no vibration) b) real.*

Focusing on the surfaces pattern created by the tool, this work investigates the spatial frequency of the surface, i.e., the inverse of the wavelength of the marks, that can be identified by applying Fourier Transform (FT) on the surface profile.

The spatial frequency content of kinematic surface is characterized by:

$$sf_{feed} = 1/f_z \tag{1}$$

where $f_z$ is the feed per tooth. Since the pattern of a machined surface, caused by harmonic tool vibrations, is periodic but not harmonic (Fig. 1), the surface spectrum will be composed by $sf_{feed}$ and harmonics. The theoretical peak to valley roughness ($R_t$) can be, instead, approximated as [18]:

$$R_t = \frac{D}{4}\frac{(\pi f_z)^2}{(2\pi \cdot D/2 + z f_z)^2} \tag{2}$$

where $D$ is the tool diameter and $z$ the number of flutes. An example of kinematic surface, simulated for $f_z$=*0.1 mm*, $D$=*8 mm* and $z$=*2* is reported in Fig. 2, along with the related surface spectrum

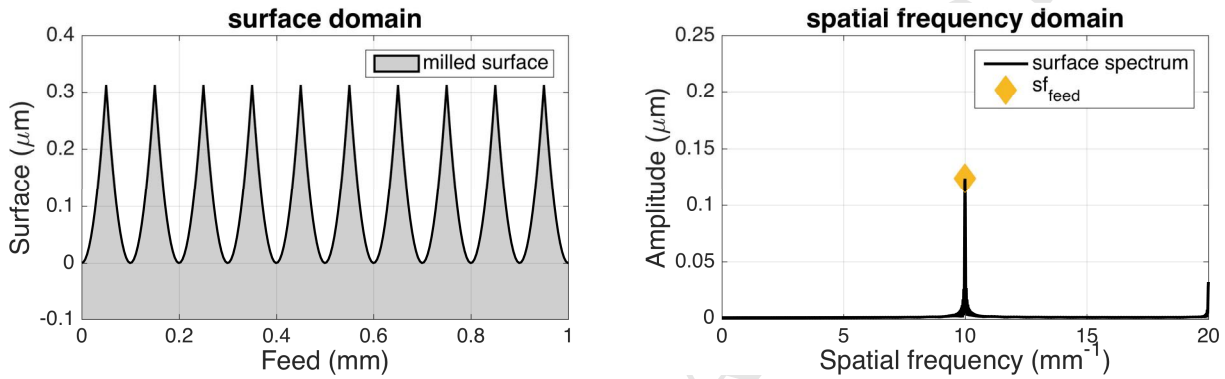


*Fig. 2 Kinematic surface marks (i.e., no vibrations) example (fz=0.1 mm).*

In an actual machining case, the tool-tip positions continuously deviate from their nominal values due to the cutter vibrations in the cross-feed direction and to the run-out (as shown in Fig. 1b), producing a great impact on the machined surface topography. From the kinematic point of view, the machined surface profile can be obtained by the cutting edges positions ($x_p$, $y_p$) at the instant in which they pass over the machined surface. This condition occurs when the cutting edge location angle (φ) becomes equal to zero for each flute engaged in the cut [19]. Based on the above definitions, the three-dimensional machined surface can be easily formed by linking the points ($x_p$, $y_p$) with arc segments, which represent the envelope of the same cutting edge trajectory of the ideal case. It is likely to think of surface profile generation as a process, where once every tooth pass instant, the tool center point displacement is "frozen" and used to locate the feed mark within the profile. The above discussion suggests that the generation of the machined profile can be regarded as a sampling process or, more specifically, as a problem of sampling (in the time domain) and reconstruction (in the spatial domain) of continuous-time signals (cutting tool displacements). Taking in mind the previously described surface generation mechanism, the sampling frequency will be the tooth pass frequency $f_{tp}$ and the Nyquist frequency will be half of it. According to the sampling theorem [20], the frequency content of a band-limited continuous periodic signal will be correctly reconstructed if the sampling frequency is above two times the maximum frequency of the original signal. Thus, limiting the analysis to the radial displacements (the most significant in affecting the machined surface), when a vibration occurs at a frequency $f_c$ in the time domain below the Nyquist frequency $f_{ny}$=$f_{tp}$/2, it will be transformed in the spatial domain according to the following equations:

$$x_t(t) = f_z f_{tp} \cdot t \tag{3}$$

$$y_t(t) = A sin(2\pi f_c \cdot t) \tag{4}$$

$$y_t(x) = \sum_{n=0}^{\infty} a_n(A) \sin\left(2\pi n \frac{f_c}{f_z f_{tp}} x\right) \tag{5}$$

where $A$ is the amplitude of the tool vibration in the cross-feed direction ($y$), $a_n$ are the Fourier coefficients of the machined surface since, even considering a purely harmonic tool vibration (i.e. only the first order Fourier coefficient), the reconstructed surface has not a harmonic pattern, i.e. it is characterized by higher order Fourier terms in the spatial frequency domain. However, according to Eq. 5, the fundamental spatial frequency content of the machined surface is related to $f_c$ according to:

$$sf_c = \frac{f_c}{f_z \cdot f_{tp}} \tag{6}$$

In Fig. 3 this condition ($f_c<f_{tp}/2$) is presented through an example in which tool vibrates at $f_c$=25 Hz, with an amplitude $A$ equal to 20 times the theoretical roughness $R_t$ (Eq. 2). The surface was reconstructed by using the tool centre position sampled at the $f_{tp}$ =100 Hz and linking the points with arc segments with radius equal to the tool (4 mm). The results in the spatial frequency domain match Eq. 6. Moreover, it highlights that despite the tool vibration is purely harmonic, the reconstructed surface has higher order harmonic terms.

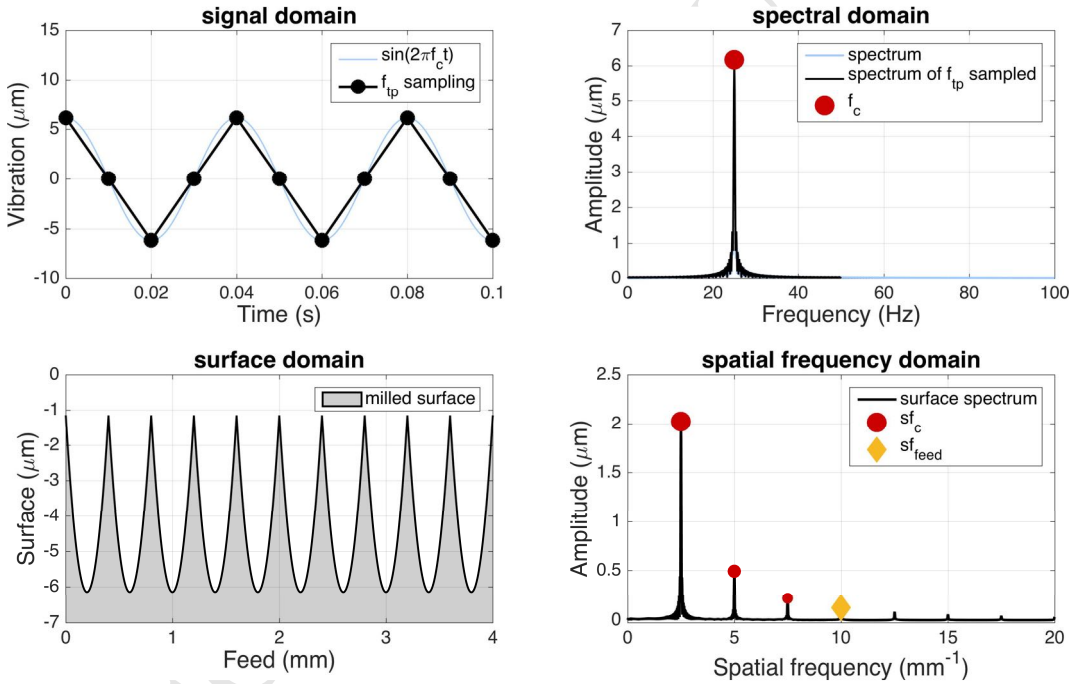


*Fig. 3 Surface waviness: frequency below $f_{tp}/2$ ($f_z$=0.1 mm, $f_c$= 25 Hz, $f_{tp}$=100 Hz, A=20Rt).*

On the other hand, the frequency contents of tool-tip vibration that do not meet the Nyquist condition ($f_c>f_{tp}/2$) will give new, false low frequencies in the sampled signal. This is due to the aliasing phenomenon. The aliased frequency $f_{c\text{-}a}$ will be related to the signal frequency $f_c$ according to the following equation [20]:

$$f_{c-a} = |f_{tp} \cdot m - f_c| \tag{7}$$

where $m$:$f_{tp}$ is the integer multiple of the tooth pass frequency (i.e., sampling frequency) which is closest to the signal frequency. This effect is clearly visible both in the signal domain (as a false low-frequency signal) and in the spectral domain (as a folded-over false low-frequency spike).
In case of forced vibrations (i.e., $f_{tp}$ and its harmonics frequency content), all the vibrations will be folded on 0 Hz values, imposing a general translation to the surface without affecting topography. On the contrary, this result has a great impact on the machined surface in case of chatter vibration,

since the chatter frequency is generally well above the tooth pass frequency and asynchronous of it, as shown in the example in Fig. 4, where tool vibration at 425 Hz is presented.

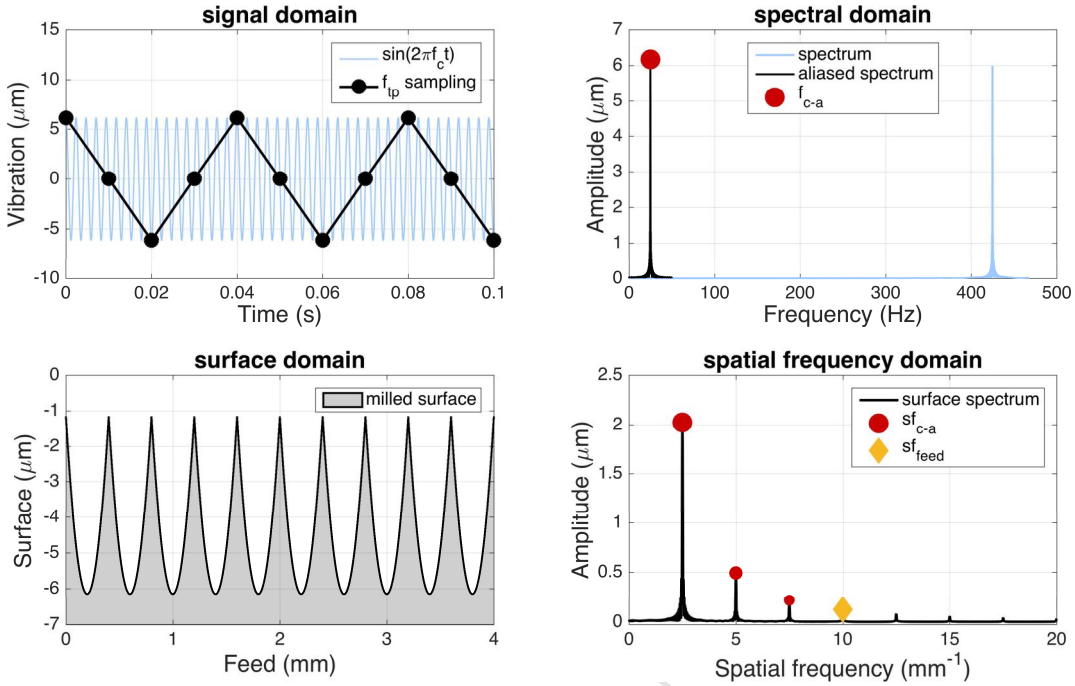


*Fig. 4 Chatter marks: aliasing effect ($f_c$= 425 Hz, $f_{tp}$=100 Hz, A=20Rt).*

According to the proposed sampling analogy, chatter frequency will be aliased, producing waviness (i.e., marks) on the machined surface characterized by spatial frequency $sf_{c-a}$:

$$sf_{c-a} = \frac{f_{c-a}}{f_z \cdot f_{tp}} = \frac{|f_{tp} \cdot m - f_c|}{f_z \cdot f_{tp}} \tag{8}$$

This is the reason why tool vibrations at high chatter frequency produce low spatial frequency marks (i.e., wide marks) on the surface. Furthermore, Eq. 8 provides a control parameter for chatter marks: theoretically no chatter marks will be produced on the machined surface whenever the chatter frequency is exactly an integer multiple of the tooth pass frequency:

$$f_{c-a} = |f_{tp} \cdot m - f_c| = 0 \qquad f_c = f_{tp} \cdot m \tag{9}$$

In addition, Eq. 8 limits the maximum value of the $sf_{c-a}$ to half of the feed marks frequency ($sf_{feed}$), which occurs when $f_{c-a}=f_{tp}/2$. In the following sections these conditions will be analyzed and discussed.

To clearly understand the generation mechanism of the chatter marks, a further phenomenon should be considered. Indeed, it is well-known in literature that some visible beating effects, often called "pseudo-moiré" effects, may also occur in the sampled signal using a sampling frequency that meets the Nyquist condition [21]. Although these effects are not aliasing consequences, they are clearly visible in the sampled signal, even if their frequencies are not represented in the Fourier spectrum. Their occurrence greatly affects the machining surface profile. The "pseudo-moiré" effects appear in the sampled signal whenever the sampling frequency $f_{tp}$ approaches (but is not equal to) an integer multiple of the aliased signal frequency $f_{c-a}$, i.e. according to the following condition:

$$f_{c-a} \approx f_{tp}/h \tag{10}$$

where $h$ is the closest integer divisor of the sampling frequency to the aliased signal frequency (i.e., order). These effects do not really correspond to a low-frequency signal, but rather to highly

oscillating signals that are only modulated by low-frequencies envelopes. Note that these low frequencies in the signal domain belong to the modulating envelopes of the sampled signal, but they are not included in the sampled signal itself.
It is possible to prove that the envelope functions highlighted in the figures are characterized by the following envelope frequencies [21]:

$$f_{pm} = \left| f_{c-a} - f_{tp}/h \right| \tag{11}$$

For what concern the machined surface profile, it must be pointed out that the chatter marks, which will be characterized by the wavelength of the aliased chatter frequency $f_{c\text{-}a}$, will be also modulated on these envelope functions in the spatial domain, characterized by the spatial frequency $sf_{pm}$:

$$sf_{pm} = \frac{h \cdot f_{pm}}{f_z \cdot f_{tp}} = \frac{h \cdot \left| f_{c-a} - f_{tp}/h \right|}{f_z \cdot f_{tp}} \tag{12}$$

This effect is, hence, not present when Eq. 11 is equal to 0, i.e., the sampling frequency $f_{tp}$ is an integer multiple of the aliased signal frequency $f_{c\text{-}a}$:

$$f_{pm} = \left| f_{c-a} - f_{tp}/h \right| = 0 \qquad f_{c-a} = f_{tp}/h \tag{13}$$

The pseudo-moiré effect is shown in the examples of Fig. 5 and Fig. 6, where 2nd and 3rd order (h) effects are presented.

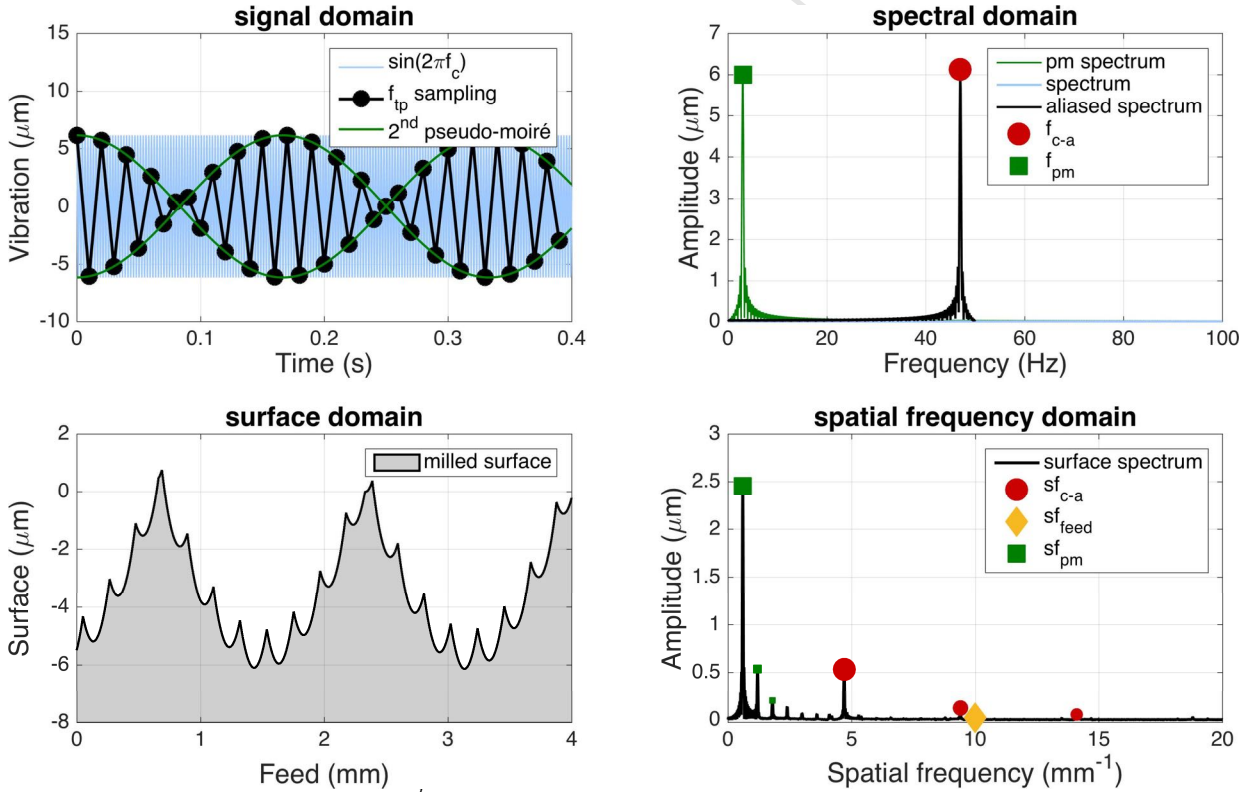


*Fig. 5 Chatter marks: 2nd order pseudo moiré effect ($f_c$= 447 Hz, $f_{tp}$=100 Hz, A=20Rt).*

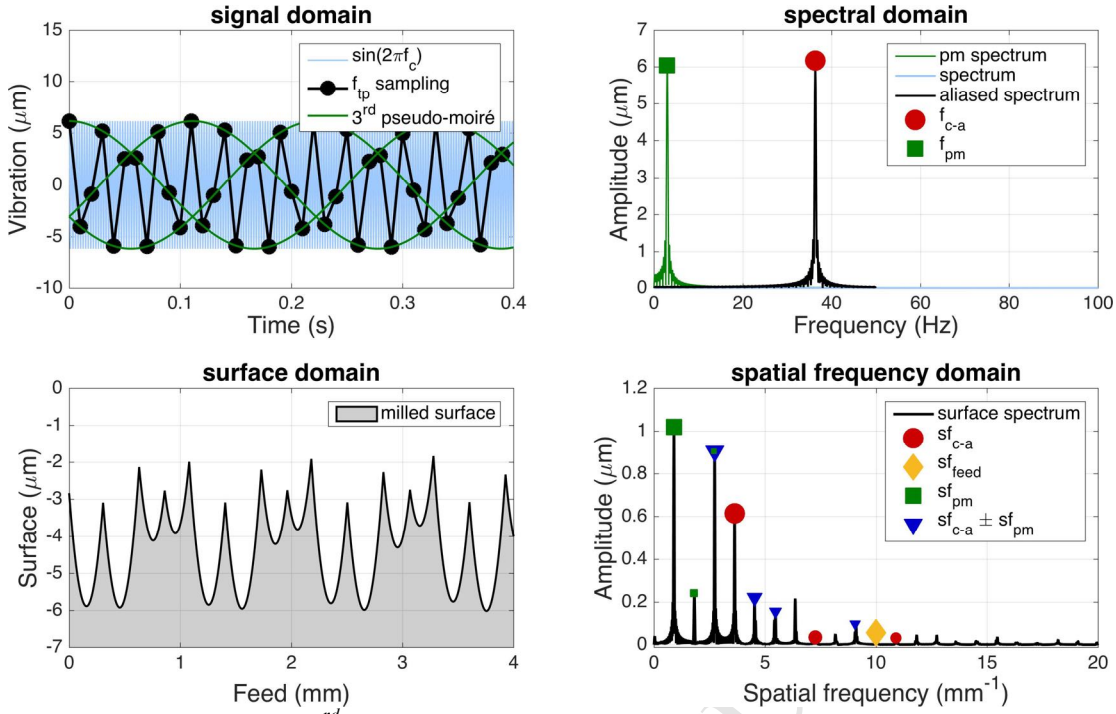


*Fig. 6 Chatter marks: 3rd order pseudo moiré effect ($f_c$= 436.33 Hz, $f_{tp}$=100 Hz, A=20Rt).*

The figures highlight that low order effects generate higher amplitude envelopes, significantly affecting the surface at the spatial frequency $sf_{pm}$. On the contrary, increasing the order, pseudo-moiré effects produce lower amplitude envelopes, reducing the influence of $sf_{pm}$ on the surface that, as consequence, presents both $sf_{c\text{-}a}$ and $sf_{pm}$, dominant on the spatial frequency spectrum. This simultaneous presence of the two effects, comparable in magnitude, results in beating effects characterized by the frequencies $sf_{c\text{-}a} \pm sf_{pm}$. This trend is confirmed by the deeper example-based investigation presented in Fig. 7b.

In addition, the influence of vibration amplitude (A) with respect to the theoretical roughness ($R_t$ eq. 2) is studied (Fig. 7a). Increasing the ratio of the vibration amplitude over the theoretical roughness, the feed marks frequency disappears from the surface spectrum. Moreover, increasing the vibration amplitude increases the influence of pseudo-moiré effects on the machined surface. This is due to the surface generation mechanism, as explained in this work (Fig. 1): since the surface is determined by the traces of the cutting edges, higher amplitude vibrations of the tool overrule smaller ones, which hence not produce significant effects on the surface. Because of this mechanism, the prediction of the surface spatial frequency spectrum is not as straightforward as the analysis of the spectrum of the time-domain tool vibration, especially for what concern amplitudes. However, relating the tool vibration frequency values (i.e., chatter frequency) to the surface spatial frequency content is crucial and sufficient to predict chatter marks pattern (i.e., spatial frequency), which is the goal of this work.

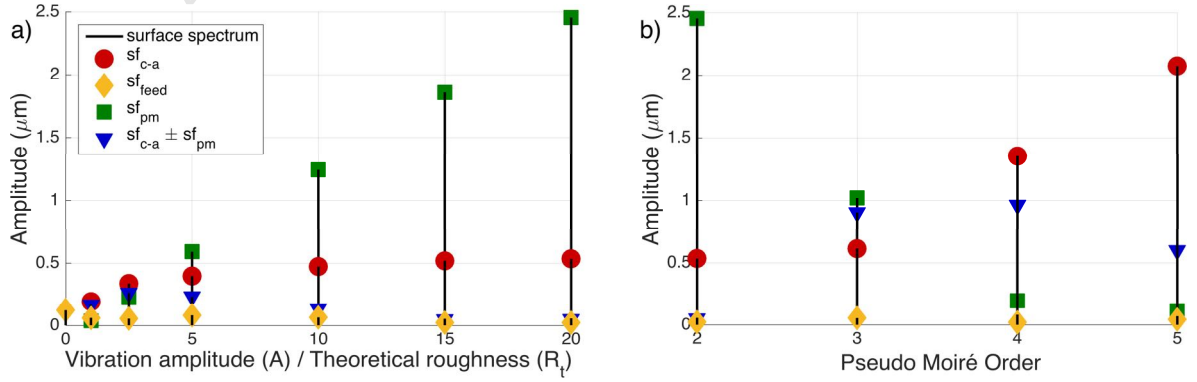


*Fig. 7 Influence of a) vibration amplitude ($f_c$=447Hz, h=2) b) pseudo moiré order (A=20Rt).*

In summary, in the most general case the spectrum in the spatial frequency domain of the chatter marks will be composed by almost two different frequencies: the aliased chatter frequency $sf_{c\text{-}a}$ and the envelope frequency $sf_{pm}$, plus the potential beating effects between the two ($sf_{c\text{-}a} \pm sf_{pm}$).

$$sf_{c-a} = \frac{|f_{tp} \cdot m - f_c|}{f_z \cdot f_{tp}} \tag{14}$$

$$sf_{pm} = \frac{h \cdot |f_{c-a} - f_{tp}/h|}{f_z \cdot f_{tp}} \tag{15}$$

## 3. NUMERICAL VALIDATION

The proposed analytical formulations, presented in the previous section, were validated through numerical simulations, composed of three main phases: i) the milled surface topography was simulated in different cutting conditions; ii) the spatial frequency spectra were then computed performing a Fourier transform of the simulated surface profile; iii) the relevant frequency contents were then compared with the values predicted by the proposed analytical formulations. This validation allowed to test the different configurations, presenting the singular effects without the influence of experimental uncertainties and noise.

### 3.1. Simulation approach

In order to investigate the characteristics of surface generated under vibrations effects, two simulation models are combined: a milled surface generation model [22] and a time-domain simulation of the milling process, as in [23]. The first one was used to compute the milled surface based on the relative displacement of tool and workpiece. The model identifies the final workpiece surface by simulating the positions of tool and cutting edges at each time step, and computing the intersection points between the cutting edges and the surface profile by using a quadratic interpolation. In the simulation, the profile points are saved in a dynamic array and continuously updated at every time step according to the material removed and the current position of the workpiece. The workpiece profile is discretized in several planes defined by their coordinates in the workpiece reference system. The algorithm requires, as input data, the time histories of the tool-workpiece relative displacements. Further details can be found in [22], similar models are also presented in [24].

In this work, tool displacements data are obtained by a time-domain simulation of the milling process, simplifying the model presented in [25]. The dynamics of the milling process, including regenerative effect, is described by a 2-dimensional linear time periodic system with a single time delay. The two degree of freedom lumped model (feed and normal directions) is excited by cutting forces on both directions computed by a mechanistic approach using instantaneous chip thickness. The system is approximately solved by using a time-domain full-discretization method based on Newmark implicit direct integration scheme.

Although this approach could be also used directly for milled surface prediction, as in [23], in this work the time-domain model was performed to extract tool-tip displacements to be used in the geometrical surface generation model. The main reason relies on flexibility and computational efficiency: storing and updating surface profile on several planes and small time-step, as required in the first approach, increases the time required for the simulation. The milled surface is hence estimated afterwards adopting arbitrary number of planes and time step.

The time-domain simulation was firstly used to reconstruct the stability lobe diagram (SLD), in a defined range of spindle speeds, for the specific configuration. Dedicated algorithms are generally used for chatter prediction, such as Zeroth Order Approximation or Semi-discretization approach [8]. However, in this case the time-domain simulation was adopted for both SLD reconstruction and milled surface generation to ensure a perfect match between the two phases, required for the selection and implementation of the cutting conditions.

The stability limits were identified by performing several process simulations, increasing the depth of cut till reaching unstable cutting condition, as in [26]. Based on the simulated SLD, several conditions were selected to highlight the different effects. For these selected conditions, the tool-tip vibrations were extracted and used as input for the milled surface generation model. The simulated surfaces were then analyzed in spectral frequency domain and compared to the frequency values predicted by the proposed formulations. The simulation approach is summarized by the block diagram presented in Fig. 8. This is the approach used for the numerical validation but it is not required in general for the application of the proposed formulation.

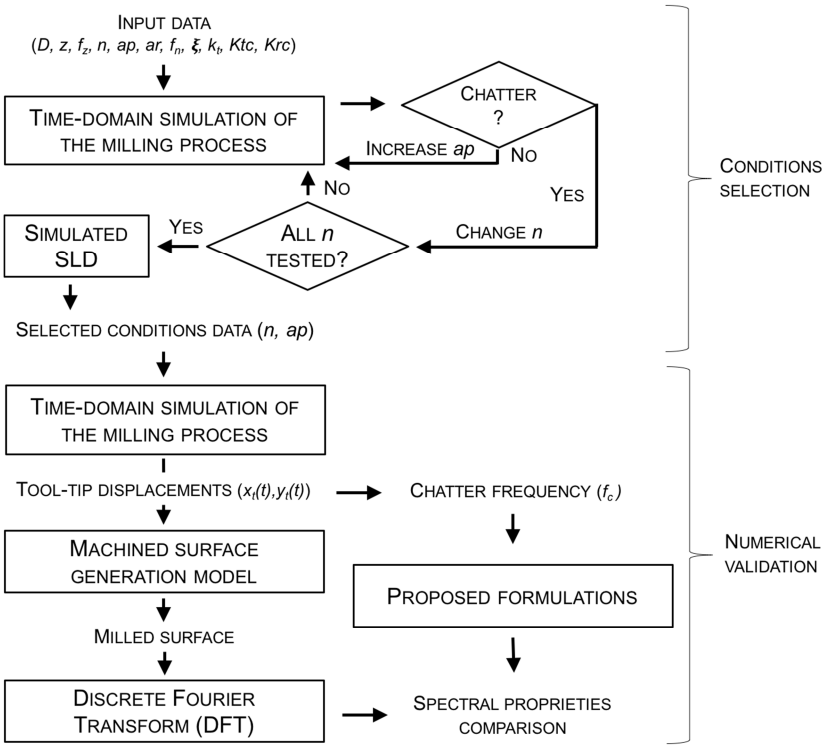


*Fig. 8 Block diagram of the proposed simulation approach for the numerical valdiation*

### 3.2. Cutting parameters and selected conditions (zero helix angle)

Simulations were carried out using the parameters of the validated test case presented in [25]. The characteristics of the tool (Garant 201320), modal parameter of the tooling system (symmetric on feed and normal directions) and process parameters (side milling on Aluminum 6072-T4) are summarized in Table 1. Tool run-out was not included in this investigation.

*Table 1. Time-domain simulation parameters.*

| Tooling | | | Tool modal parameters | | | Cutting parameters | | | | Cutting force coefficients | |
|---|---|---|---|---|---|---|---|---|---|---|---|
| Helix angle (°) | Diameter (mm) | z | $f_n$ (Hz) | $\xi$(%) | $k_t$ (N/m) | ar (mm) | ap (mm) | n (rpm) | $f_z$ (mm) | Ktc (N/mm$^2$) | Krc (N/mm$^2$) |
| 0 | 10 | 2 | 1836.6 | 2.31 | 1.15e7 | 2 | 3.5-7 | 2520-2616 | 0.1 | 1086.7 | 139.0 |

As previously mentioned, SLD was simulated (Fig. 9) to support the selection of cutting conditions. For the identification, the depth of cut resolution was set to 0.02 mm and chatter onset was detected based on the amplitude spectrum of tool-tip displacement, i.e. checking when a dominant frequency (i.e., chatter frequency) exceeds the amplitude of tooth pass frequency (Fig. 9a). This chatter detection approach excludes the transition phase in which chatter occurs but it is not dominant on the spectra, however the approximation was considered valid, since the goal was to identify the full-developed chatter.

Computed chatter frequencies (Fig. 9b) were processed via Eq. 14 and 15 to predict the resulting spatial frequencies, (shown in Fig. 9c). This allowed to detect the general trend of chatter marks

pattern changing with spindle speed, according to the proposed analytical formulations, and to select significant configurations to be used for the validation. In the specific case (Fig. 9c), within the same lobe, $sf_{c\text{-}a}$ increases up to its maximum allowable value (half of the feed marks spatial frequency $sf_{feed}$) and decreases again. On the other hand, $sf_{pm}$ increases and decreases multiple times, since $f_{c\text{-}a}$ reaches different submultiples of the $f_{tp}$ (different $h$).

As shown in Fig. 9b, chatter frequency varies between multiples of tooth pass frequency without reaching them; therefore, the singular condition presented in Eq. 9 for which marks are not generated, cannot be fulfilled according to chatter predictive theory. Therefore, chatter vibrations always leave distinctive marks on the surface. On the other hand, the condition depicted in Eq. 13 can occur, resulting in the absence of pseudo-moiré effects at specific spindle speeds.

Based on the computed SLD, 12 conditions were selected on a single lobe (stars in Fig. 9a). This selection includes:

- stable and unstable cutting with increasing vibration (i.e., increasing depth of cut);
- conditions in which the proposed formulations predict an absence of pseudo-moiré effects (2520 and 2602 rpm) to validate Eq. 13;
- conditions with predicted pseudo-moiré effects of different order, to check its influence;
- condition between lobes (2614 and 2616 rpm), to study the influence of the chatter frequency discontinuity.

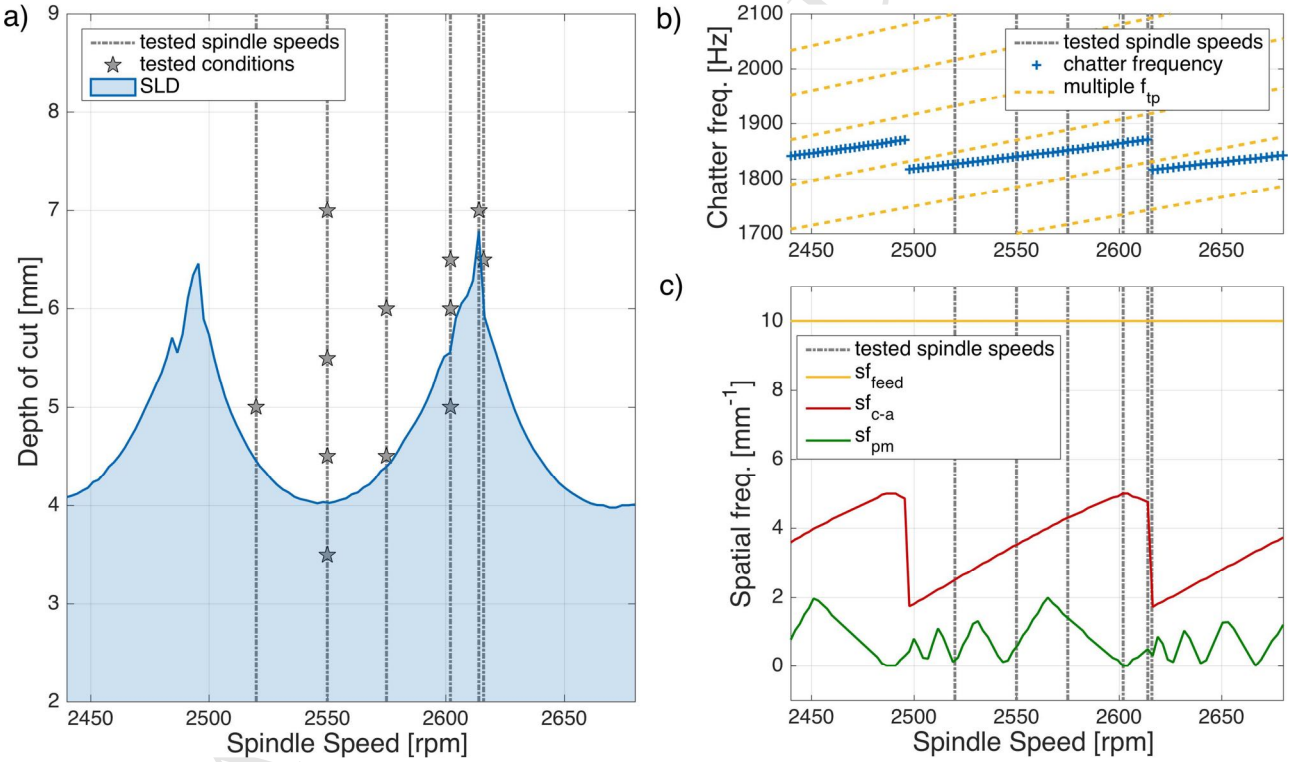


*Fig. 9 Simulated SLD with selected conditions for the numerical validation: a) depth of cut, b) chatter frequency, c) predicted chatter marks spatial frequencies.*

***Results and discussion***

The tool-tip displacements computed by the time-domain model in the selected configurations, were used as inputs for the milled surface generation simulator to predict the flank surfaces (feed-tool axis plane). The time step of the milled surface simulation was set to discretize the tool rotation period in 800 intervals, ensuring 10 points per feed per tooth. The calculated surfaces were analyzed in the spatial frequency domain by applying DFT (Discrete Fourier Transform) on the surface profile, extracted at a defined depth, conviniently windowed and detrended of its average value. Since a zero-helix tool is simulated, the surface profile is not changing along z axis. The following

figures (Fig. 10-Fig. 16) show the simulated surfaces (on the left) and the spatial frequency analysis (on the right), in which the spectrum of the surface (black line) is compared with the spatial frequency values predicted by the proposed analytical formulation (colored markers).
Fig. 10 shows the predicted surface for a stable condition (2550 rpm and ap=3.5 mm). In this case, the generated surface is characterized by a waviness spaced of $f_z$ as in the ideal condition (Eq. 1). Indeed, forced vibrations (multiples of the tooth pass frequency) result in a null $sf_{c\text{-}a}$, producing only a constant surface error. In the frequency analysis, $f_{feed}$ (10 mm$^{-1}$) and its harmonics are found, as expected.

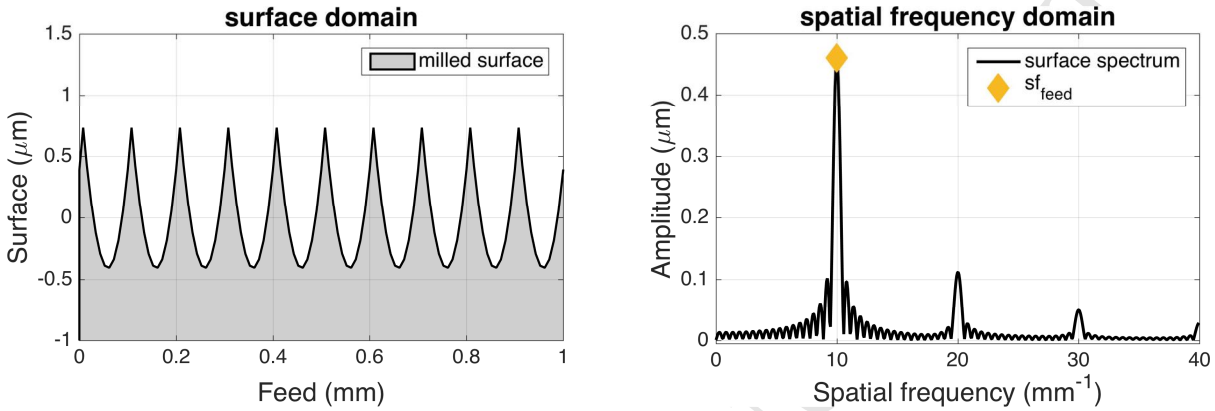


*Fig. 10 Surface profile and spatial spectra for 2550 rpm and 3.5 mm depth of cut.*

Increasing the depth of cut, chatter vibrations occur and surface shows chatter marks, as presented in Fig. 11 for the 2550 rpm and ap=5.5 mm condition, characterized by a chatter frequency of about 1840 Hz. As predicted by Eq. 14 and 15, two main contributions are identified on the chatter marks surface: the waviness caused by the aliased chatter frequency ($sf_{c\text{-}a}$) is coupled with the one caused by the 3rd order pseudo-moiré effect ($sf_{pm}$). Beating effects between the two ($sf_{c\text{-}a} \pm sf_{pm}$) and harmonics are also found. The spatial frequency domain comparison highlights the accuracy of the proposed formulations in predicting the surface frequency content.

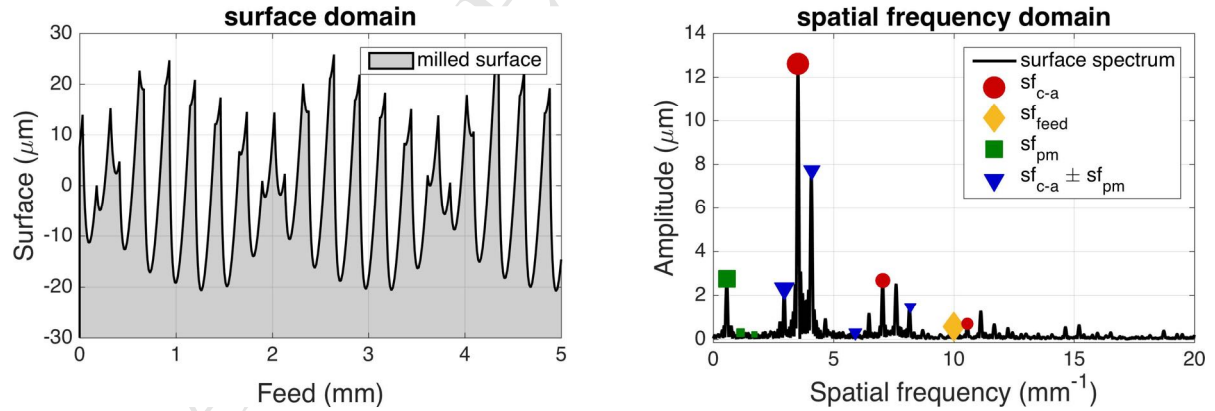


*Fig. 11 Surface profile and spatial spectra for 2550 rpm and 5.5 mm depth of cut ($f_c$=1840 Hz, h=3).*

Further increasing the depth of cut to 7 mm (Fig. 12) results in an increase of the vibrations amplitude at the same chatter frequency (1840 Hz). Therefore, the same two contributions are found on the surface, but the influence of pseudo-moiré effect ($sf_{pm}$) increases, as expected from the trend identified by the analysis shown in Fig. 7a.

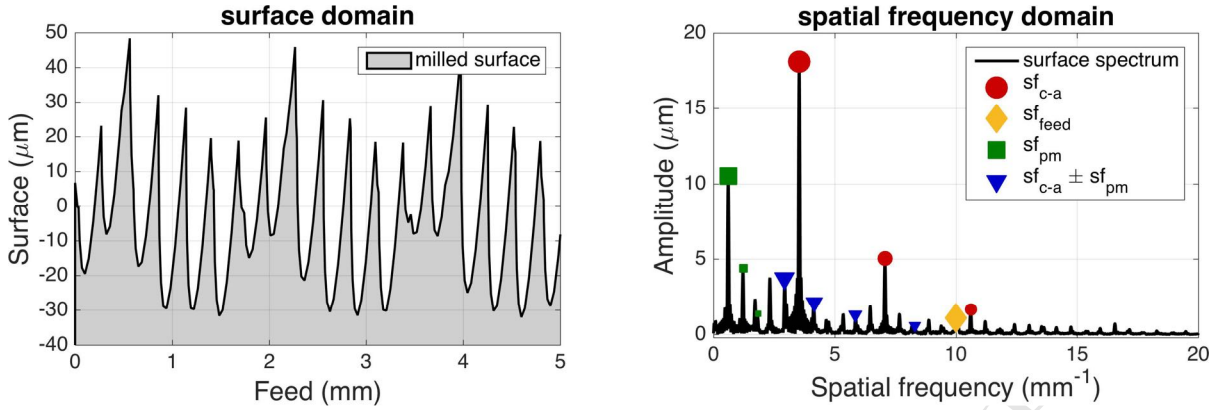


*Fig. 12 Surface profile and spatial spectra for 2550 rpm and 7 mm depth of cut ($f_c$=1840 Hz, h=3).*

As previously mentioned, at 2520 and 2602 rpm, the condition of Eq. 13 is fulfilled, i.e., aliased frequency ($f_{c\text{-}a}$) is sub-synchronous of the $f_{tp}$. In the 2520 rpm case, the proposed formulations predict that pseudo-moiré effect disappears, leading to a surface wavelength multiple of the feed per tooth ($f_z$). This is confirmed by the simulated surfaces, as shown in Fig. 13 where the condition of $f_a$ equal to $f_{tp}$/4 is shown (2520 rpm and $f_c$=1827 Hz, ap=5 mm). For this specific case, the surface profile is characterized by a dominant frequency equal to a fourth of the $sf_{feed}$, as predicted by Eq. 14.

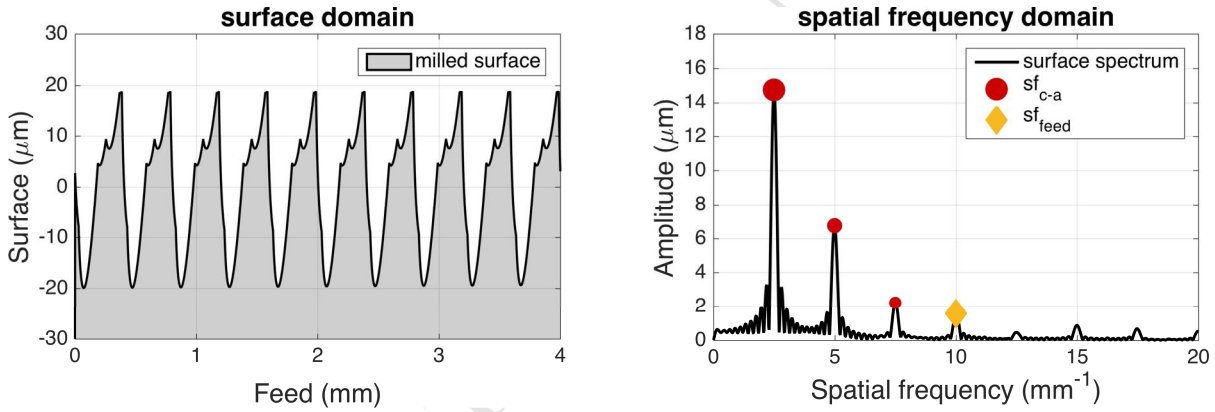


*Fig. 13 Surface profile and spatial spectra for 2520 rpm and 5 mm depth of cut ($f_c$=1827 Hz, h=4).*

The same considerations can be drawn for the second test condition (2602 rpm and $f_c$=1864.7 Hz, ap=6 mm), in which a dominant spatial frequency equal to half of the $sf_{feed}$ is found as expected (Fig. 14). No other significant contributions are identified in the frequency content of the profiles.

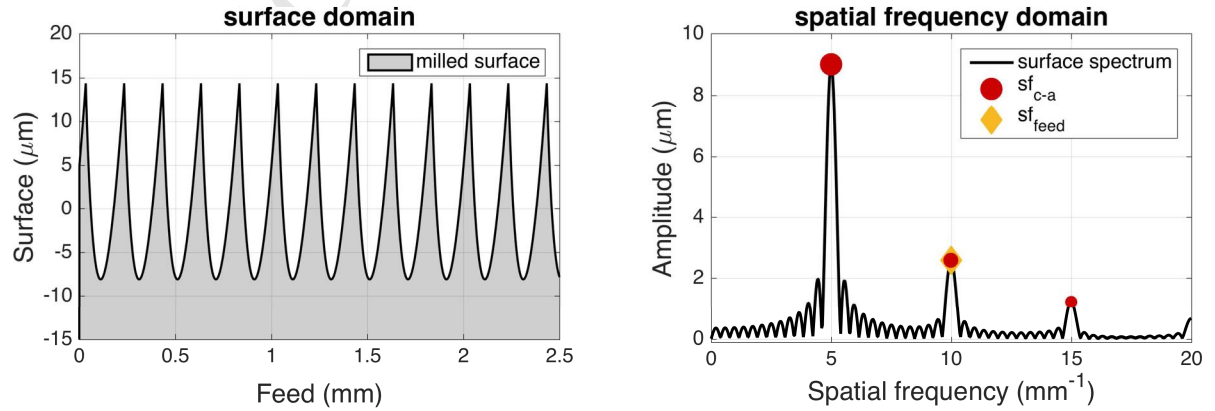


*Fig. 14 Surface profile and spatial spectra for 2602 rpm and 6 mm depth of cut ($f_c$=1864.7 Hz, h=2).*

In addition, it is interesting to point out that a small variation of the spindle speed can drastically change the chatter frequency, and hence the chatter marks pattern. An example of this effect is

represented by the lobe transition, tested in the numerical validation with the 2614 and 2616 rpm conditions (Fig. 15 and Fig. 16 respectively).

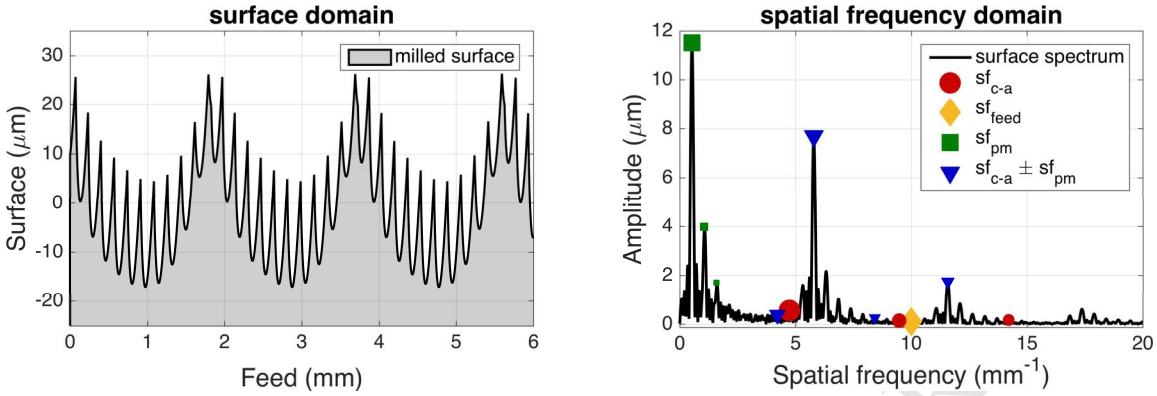


*Fig. 15 Surface profile and spatial spectra for 2614 rpm and 7 mm depth of cut ($f_c$=1871.1 Hz, h=2).*

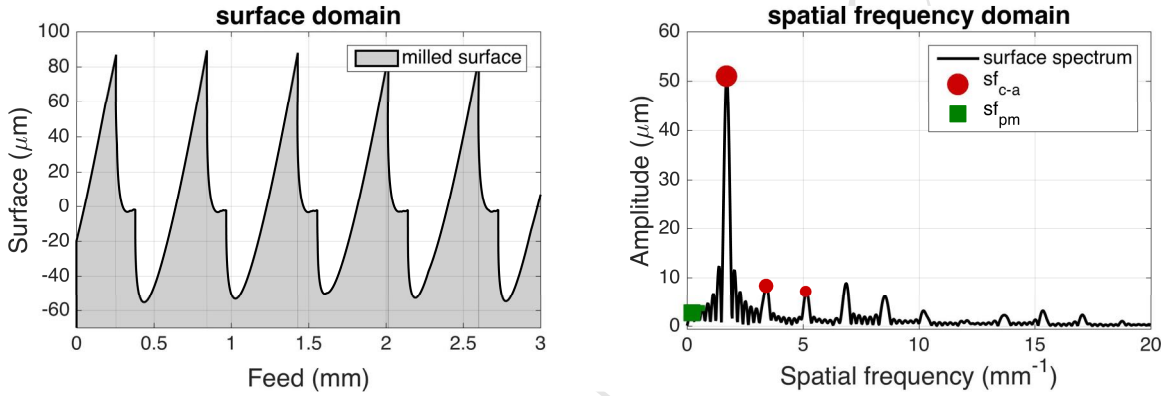


*Fig. 16 Surface profile and spatial spectra for 2616 rpm and 6.5 mm depth of cut ($f_c$=1816.4 Hz, h=6).*

It is clear from the figures that the change in chatter frequency (from 1871.1 Hz to 1816.4 Hz) results in a significant change of the chatter marks pattern. On one hand, at 2614 rpm the surface is dominated by large waviness (low spatial frequency) caused by pseudo moiré effects. On the other hand, at 2616 rpm the surface is almost only composed by the effect of aliased frequency ($sf_{c\text{-}a}$). These results confirm the influence of pseudo moiré effects order ($h$) on the surface profile, as already presented in Fig. 7b: increasing the order, the $sf_{pm}$ contribution decreases, leading to negligible influence at high orders.

The outcomes of the numerical investigation are presented in Table 2, which summarizes the predicted values by the proposed analytical formulations (Eq. 14 and Eq. 15) and the main dominant spatial frequencies on the simulated surfaces (numerical results) for each tested configuration. Comparisons of these two outcomes confirm the accuracy of the proposed formulations in predicting the main dominant frequency contributions on the surfaces using $sf_{c\text{-}a}$ (in red) and $sf_{pm}$ (in green).

*Table 2. Surface simulations results.*

| Simulation values | | | | | Proposed formulations prediction | | | | Simulated surfaces analysis | | | |
|---|---|---|---|---|---|---|---|---|---|---|---|---|
| Condition (C=chatter S=stable) | n (rpm) | $f_{tp}$ (Hz) | ap (mm) | $f_c$ (Hz) | $f_{c\text{-}a}$ (Hz) | $f_{feed}$ ($mm^{-1}$) | $sf_{c\text{-}a}$ ($mm^{-1}$) | $sf_{pm}$ ($mm^{-1}$) | Spatial frequency dominant contributions ($mm^{-1}$) | | | |
| C – No pseudo-moiré | 2520 | 84 | 5 | 1827.0 | 21.0 | 10.0 | **2.50** | 0 | *2.50* | 5.00 | 7.50 | 10.0 |
| S | 2550 | 85 | 3.5 | - | - | 10.0 | - | - | 10.0 | 20.0 | 30.0 | |
| C – h=3 | 2550 | 85 | 4.5 | 1840.0 | 29.9 | 10.0 | **3.50** | **0.55** | *0.55* | 2.95 | *3.50* | 4.05 |
| C – h=3 | 2550 | 85 | 5.5 | 1840.0 | 29.9 | 10.0 | **3.50** | **0.55** | *0.55* | 2.95 | *3.50* | 4.05 |
| Severe C – h=3 | 2550 | 85 | 7 | 1840.0 | 29.9 | 10.0 | **3.50** | **0.55** | *0.55* | 2.95 | *3.50* | 4.05 |
| C – h=2 | 2575 | 85.8 | 4.5 | 1851.3 | 37.0 | 10.0 | **4.30** | **1.38** | *1.38* | 2.85 | *4.31* | |
| C – h=2 | 2575 | 85.8 | 6 | 1851.3 | 37.0 | 10.0 | **4.30** | **1.38** | *1.38* | 2.85 | *4.31* | |
| S | 2602 | 86.7 | 5 | - | - | 10.0 | - | - | 10.0 | 20.0 | 30.0 | |
| C - No pseudo-moiré | 2602 | 86.7 | 6 | 1864.7 | 43.3 | 10.0 | **5.00** | 0 | *5.00* | 10.0 | 15.0 | 20.0 |
| C - No pseudo-moiré | 2602 | 86.7 | 6.5 | 1864.7 | 43.3 | 10.0 | **5.00** | 0 | *5.00* | 10.0 | 15.0 | 20.0 |
| C – h=2 | 2614 | 87.1 | 7 | 1871.1 | 41.3 | 10.0 | **4.70** | **0.53** | *0.53* | 1.06 | 5.78 | 6.31 |
| C – h=6 | 2616 | 87.2 | 6.5 | 1816.4 | 14.8 | 10.0 | **1.70** | **0.21** | *1.70* | 3.40 | 5.10 | |

**Green bold:** pseudo moiré predicted *Green italic:* pseudo moiré simulated
**Red bold:** aliased predicted *Red Italic:* aliased simulated

## 4. EXPERIMENTAL VALIDATION

The proposed method, validated on the simulated surfaces, was tested on an experimental case study. Side milling tests of an aluminum alloy were carried out carried out on a Mori Seiki NMV1500DCG machine. A single fluted tool (Garant 201040) was used to avoid run-out influence [5]. The cutting conditions and parameters are summarized in Table 3.

*Table 3. Experimental parameters*

| Material | Tool | D (mm) | Helix (°) | $f_z$ (mm) | n (rpm) | z | ar (mm) | ap (mm) | $f_n$ (Hz) |
|---|---|---|---|---|---|---|---|---|---|
| Al6072-T4 | Garant 201040 | 8 | 26 | 0.03 | 6950-7200 | 1 | 2 | 8 | 4560 |

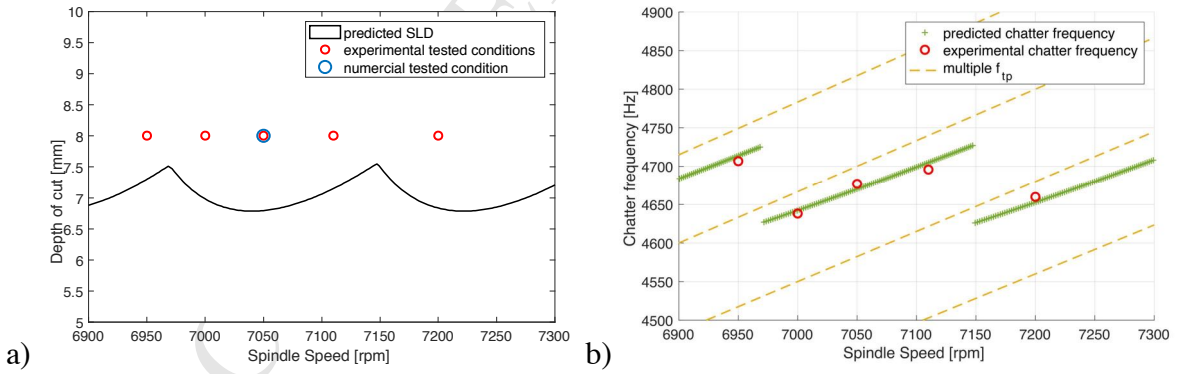


a) b)

*Fig. 17 Simulated SLD with selected conditions for experimental validation: a) depth of cut, b) chatter frequency.*

First, to select suitable cutting conditions, the SLD was computed (Fig. 17a), as in the numerical validation section. Cutting force coefficients were identified using the mechanistic approach (Ktc=1148.2 MPa Krc=786.2 MPa) and tool-tip FRFs were acquired using the impact testing technique. Based on the simulated SLD, five chatter conditions were selected: 3 within a single lobe and two on the adjacent ones, with the aim of checking the transition.

### 4.1. Numerical test

Before performing the experimental tests, a further numerical analysis was carried out to investigate the proposed formulations in case of helix angle. The same approach adopted in the previous section was performed for the condition of 7050 rpm and 8 mm depth of cut. Since the helix angle is not zero, the surface changes along z axis, therefore surface profiles at three different depths of

cut (0, 4 and 8 mm) are presented. Fig. 18, Fig. 19 and Fig. 20 show the resulting surfaces and the frequency analysis, as in the previous section.

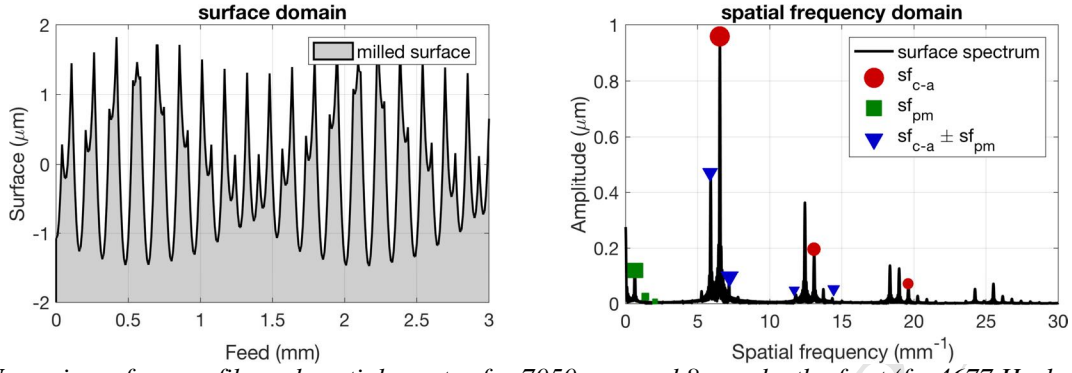


*Fig. 18 Numeric surface profile and spatial spectra for 7050 rpm and 8 mm depth of cut ($f_c$=4677 Hz, h=5), acquired depth 0 mm.*

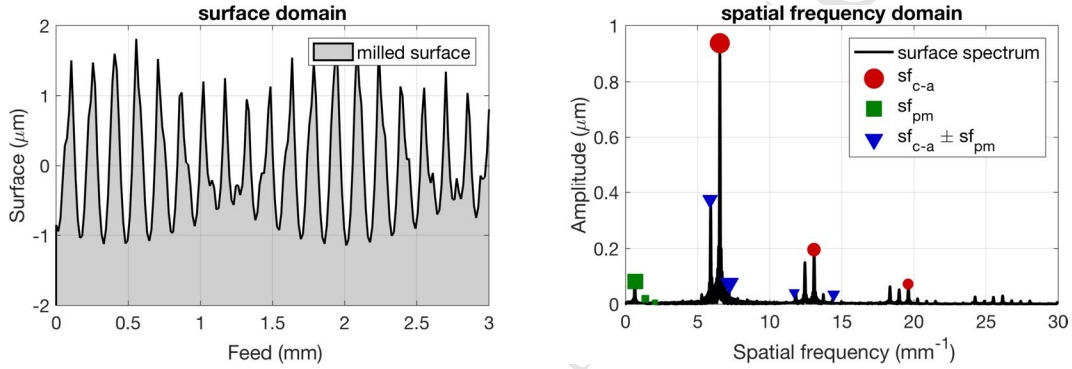


*Fig. 19 Numeric surface profile and spatial spectra for 7050 rpm and 8 mm depth of cut ($f_c$=4677 Hz, h=5), acquired depth 4 mm.*

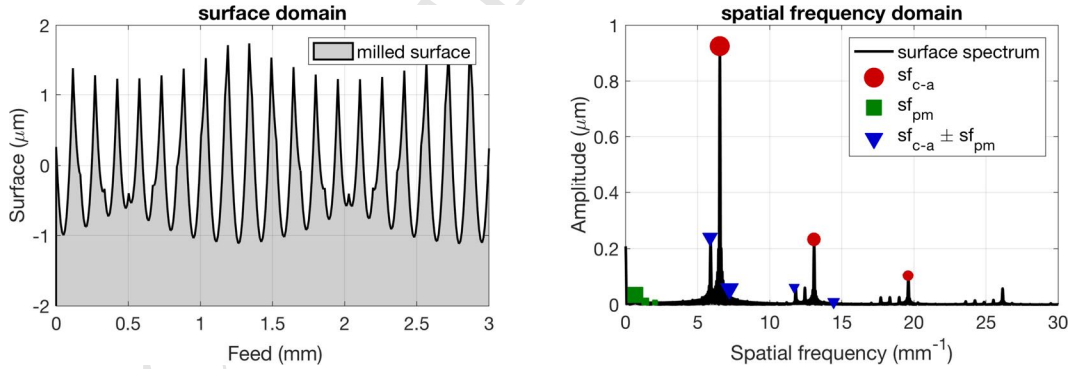


*Fig. 20 Numeric surface profile and spatial spectra for 7050 rpm and 8 mm depth of cut ($f_c$=4677 Hz, h=5), acquired depth 8 mm.*

The results show how the proposed analytical formulations accurately predict surfaces generated by tool with helix angle. Chatter marks are distributed with the same spatial frequencies at the different levels, equal to the predicted values ($sf_{c\text{-}a}$ and $sf_{pm}$). The helix angle induces only a shift of the marks respect to the position on the feed direction. The micro-topography of the surface (i.e., the marks on the surface) does not depend on helix angle, that on the contrary influences the macro-topography (i.e., SLE), as explained in [7]. The chatter marks distribution, focus of this work, is governed mainly by the tool vibration frequency (i.e., chatter frequency) and can be described by the proposed generation mechanism.

### 4.2. Experimental tests

The selected five conditions previously presented were tested on the machine tool. During cutting operations, the signal of a microphone (GRAS 46AQ) and a tri-axial accelerometer (PCB 356A32) on the spindle base were acquired, compensated [27] and analyzed to identify chatter frequency values. The machine set-up is presented in Fig. 21a.

The resulting surfaces were scanned using a Mahr C3A roughness tester equipped with RFHTB50e touch probe (Fig. 21b). Because of the probe size, only one surface line was acquired for each test case at about 4 mm depth. Surface profiles acquired were filtered and analyzed in the spatial frequency domain via DFT, as for the numerical surfaces. Resulting spectra were compared with the proposed analytical formulations outcomes (identified via markers, as in the previous analysis), to assess the accuracy of the proposed approach.

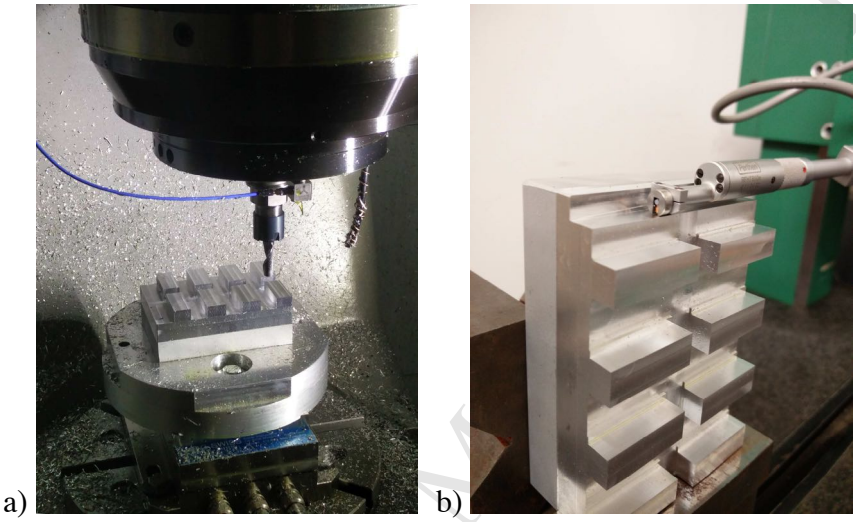

*Fig. 21 Experimental set-up: a) milling test b) roughness measurement.*

The surface obtained at 7050 rpm (Fig. 22) presents a dominant spectral frequency (6.55 $mm^{-1}$), accurately predicted by the proposed formulation ($sf_{c\text{-}a}$=6.53 $mm^{-1}$, error 0.3%) In addition, the 5th order pseudo-moiré effects ($sf_{pm}$ and harmonics) are found with lower amplitude. Milled surface acquired by the roughness tester (Fig. 22 on the left) was compared with the simulated surface presented on the previous section (Fig. 20): results show a good agreement, especially for the marks distribution, validating the numerical analysis.

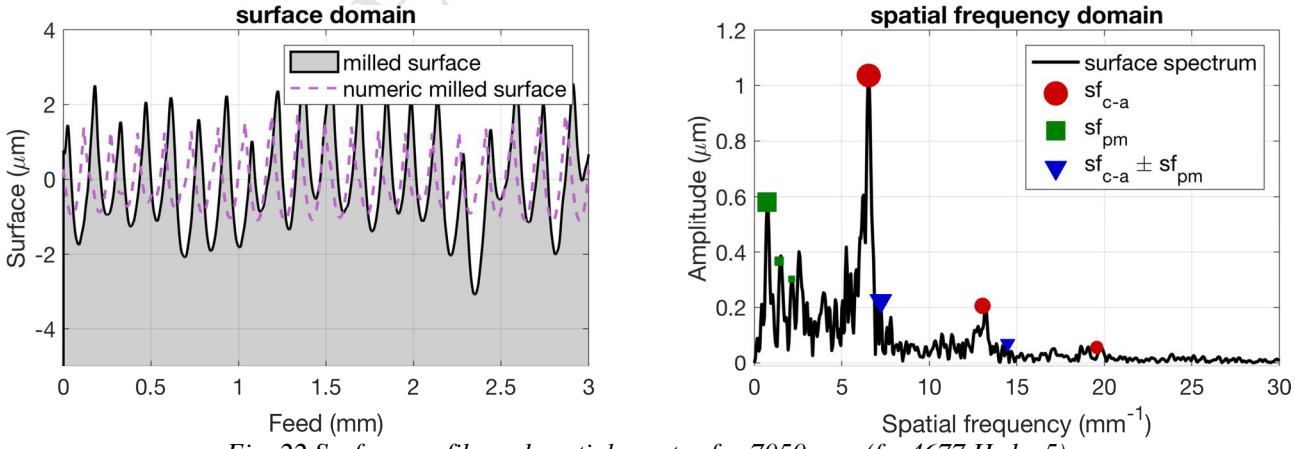


*Fig. 22 Surface profile and spatial spectra for 7050 rpm ($f_c$=4677 Hz h=5).*

Analyzing the spectrum of the 7000 rpm surface (Fig. 23) the contribution of the $sf_{pm}$ and its harmonics is higher than the $sf_{c\text{-}a}$ one. This is due to the lower order of the pseudo moiré effects ($h$=4). Additionally, contributions at around 8 $mm^{-1}$, close to the predicted $f_{c\text{-}a}$ (8.15 $mm^{-1}$), can be

identified, consisting in two dominant frequencies are found equal to about 7.3 and 8.9 mm$^{-1}$. These frequencies are probably caused by the beating effects between $sf_{c\text{-}a}$ and $sf_{pm}$ generated on the surface, since the two frequencies are equal to the sum and the difference of the predicted $sf_{c\text{-}a}$ and $sf_{pm}$.

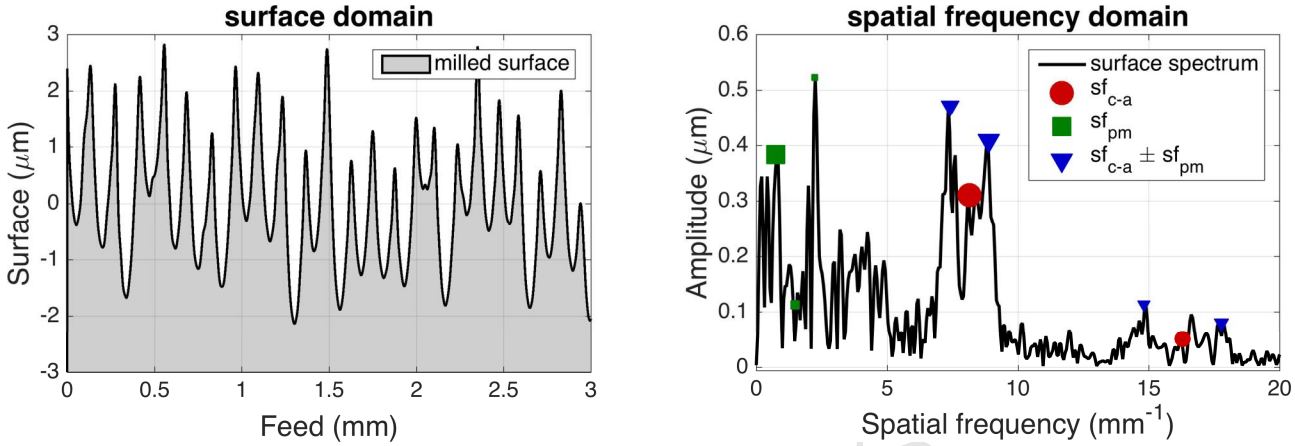


*Fig. 23 Surface profile and spatial spectra for 7000 rpm ($f_c$=4638 Hz h=4).*

Similar considerations could be drawn for the surface at 7200 rpm (Fig. 24), although at higher $h$, the influence of pseudo moiré effects is lower and $sf_{c\text{-}a}$ and beating effects are dominant, in accordance to the numerical results. The spectral proprieties are accurately predicted by the proposed analytical formulations with errors below 0.03 mm$^{-1}$.

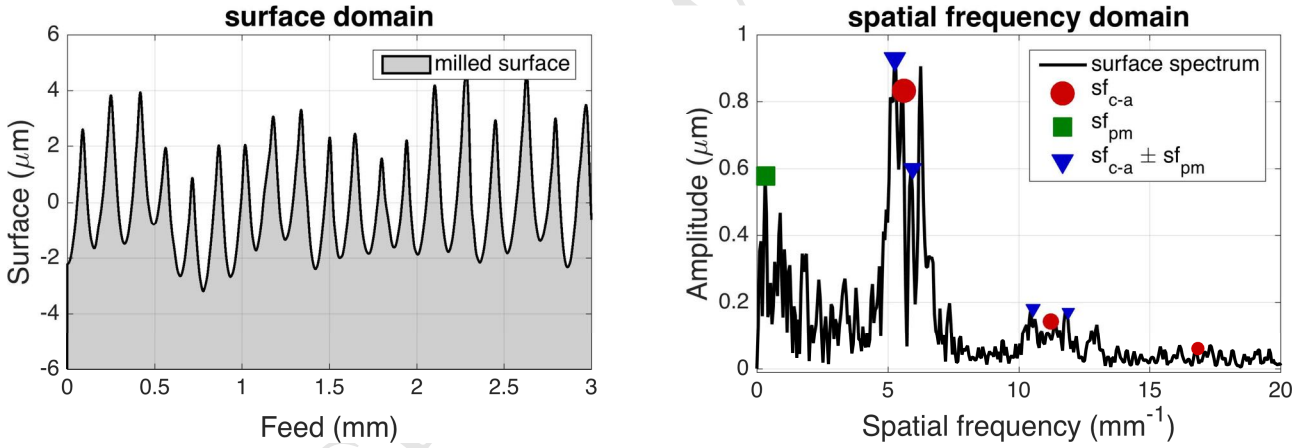


*Fig. 24 Surface profile and spatial spectra for 7200 rpm ($f_c$=4660 Hz h=6).*

In the surface at 6950 rpm (Fig. 25), a frequency (3.35 mm$^{-1}$), accurately predicted by proposed formulation for $sf_{pm}$ (3.33 mm$^{-1}$), overwhelm any other contributions. This is due to the low order ($h$) of the pseudo-moiré effect ($h$=3), which leads to a great impact of $s_{fpm}$ on the surface (Fig. 25). $sf_{c\text{-}a}$ cannot be found in the surface spectrum even if, in some parts of the surface profile, small waviness of about 0.083 mm (spatial frequency 12.1 mm$^{-1}$) are observed, close to the predicted value (12.2 mm$^{-1}$).

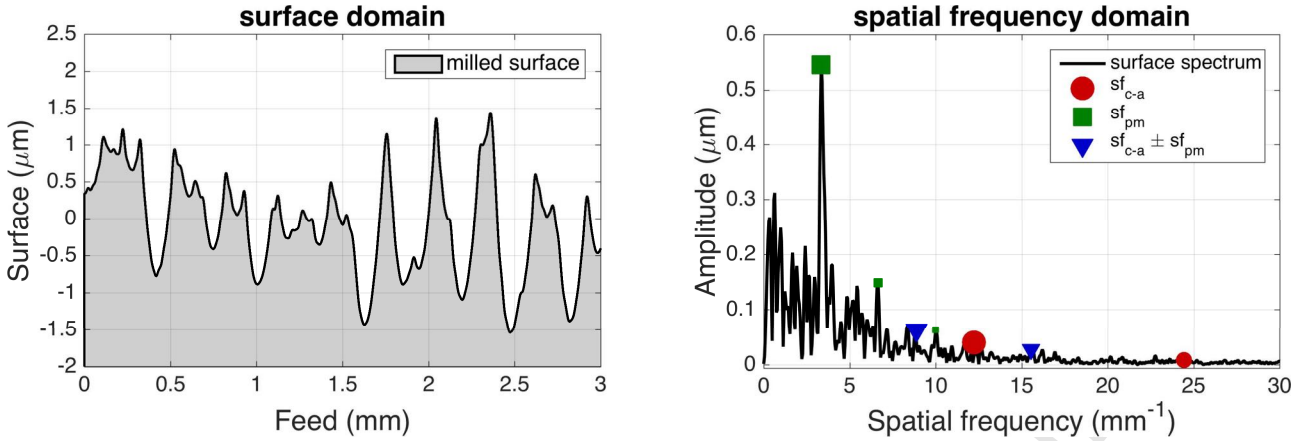


*Fig. 25 Surface profile and spatial spectra for 6950 rpm ($f_c$=4707 Hz, h=3).*

As expected, same trends are obtained for the surface at 7110 rpm (Fig. 26), i.e. a similar point on the next lobe, in which the low order pseudo moiré effect ($h$=3) is the main contribution on the surfaces profile. The spatial frequency value of this contribution is accurately predicted by Eq. 15, with small error (about 0.3%).

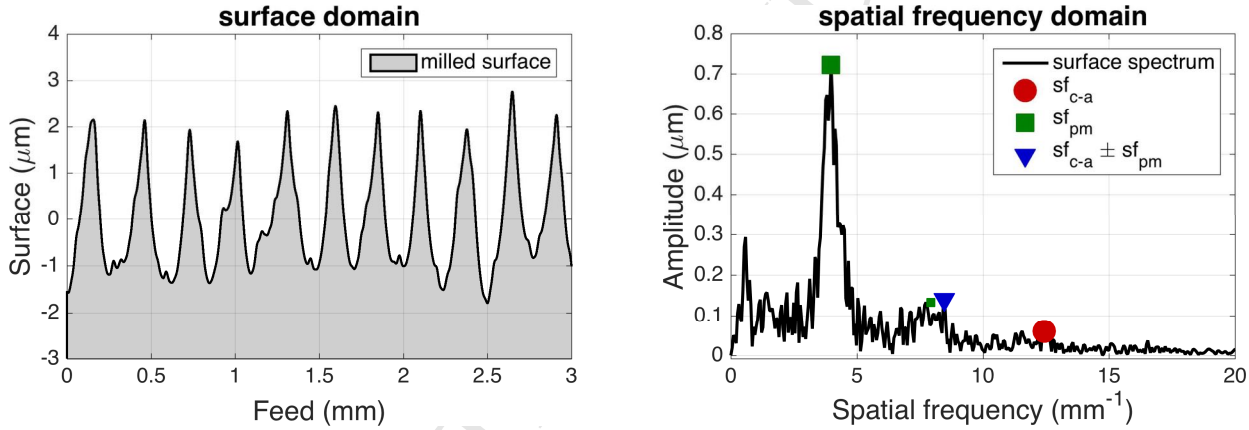


*Fig. 26 Surface profile and spatial spectra for 7110 rpm ($f_c$=4696 Hz, h=3).*

For all the presented conditions, the proposed formulations accurately predict the spatial frequency content of the surface, as summarized in Table 4, where the main dominant frequencies of the experimental surfaces are reported and compared with the frequency values predicted by the proposed analytical formulations ($sf_{c\text{-}a}$ in red and $sf_{pm}$ in green).

*Table 4. Experimental surface results.*

| Simulation values | | | | | | Proposed formulations prediction | | | | Experimental surfaces analysis | | | |
|---|---|---|---|---|---|---|---|---|---|---|---|---|---|
| n (rpm) | z | $f_{tp}$ (Hz) | ar (mm) | ap (mm) | $f_c$ (Hz) | $f_{c\text{-}a}$ (Hz) | $f_{feed}$ ($mm^{-1}$) | $sf_{c\text{-}a}$ ($mm^{-1}$) | $sf_{pm}$ ($mm^{-1}$) | Spatial frequency dominant contributions ($mm^{-1}$) | | | |
| 6950 | 1 | 115.8 | 2 | 8 | 4706.7 | 42.5 | 33.3 | **12.20** | **3.33** | *3.35* | 6.65 | 9.99 | |
| 7000 | 1 | 116.7 | 2 | 8 | 4638.2 | 28.5 | 33.3 | **8.15** | **0.74** | *0.78* | 2.30 | 7.30 | 8.86 |
| 7050 | 1 | 117.5 | 2 | 8 | 4677.0 | 23.0 | 33.3 | **6.53** | **0.71** | *0.73* | 1.50 | 2.20 | *6.55* |
| 7110 | 1 | 118.5 | 2 | 8 | 4695.8 | 44.2 | 33.3 | **12.40** | **3.97** | 0.58 | *3.98* | 8.48 | |
| 7200 | 1 | 120.0 | 2 | 8 | 4659.8 | 20.2 | 33.3 | **5.61** | **0.33** | *0.32* | 5.26 | *5.58* | 5.89 |

**Green bold:** pseudo moiré predicted *Green italic:* pseudo moiré experimental
**Red bold:** aliased predicted *Red Italic:* aliased experimental

### 4.3. Experimental surfaces

Since the probe size limits the surface investigation along tool axis, an image analysis of surfaces photos was included in the study. The five surfaces photos in b/w are presented in Fig. 27, along with a zoom, performed on the part of the photos in which marks are clearly visible.

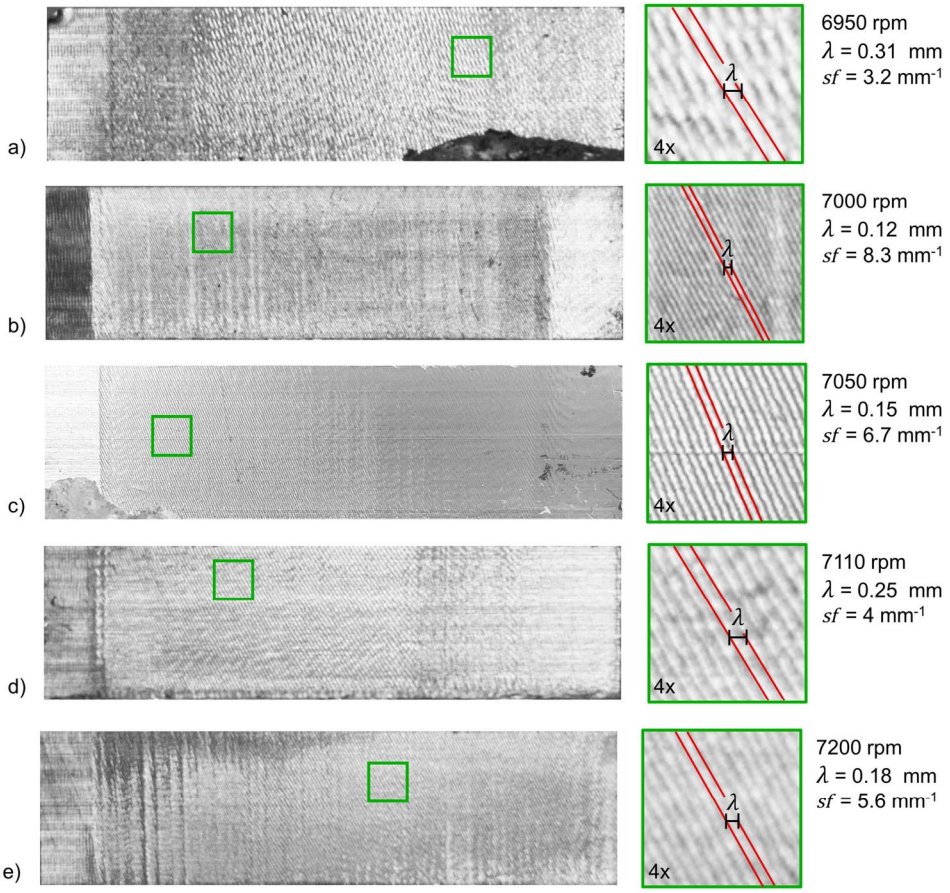


*Fig. 27 Surface photos, with zoom and analysis a) 6950 rpm b) 7000 rpm c) 7050 rpm d) 7110 rpm e) 7200 rpm*

Surfaces photos show chatter marks on the surfaces except for the beginning and ending parts, in which chatter does not occur (entry and exit phases). Although the marks are oblique along tool axis due to the helix angle, their distribution on feed direction appears constant.

Zooms were further analyzed to extract an estimated value of wavelength (λ), as presented in Fig. 27. The results of this analysis confirm the outcomes of the roughness measurements: spatial frequencies (*sf*) related to such dominant wavelengths are close to the predicted values (Table 4). Obviously, the image analysis, as reported in this work, is not accurate as the analysis performed by roughness tester, and it is provided as supplementary macroscopic validation to show the chatter marks on the entire surface, both along feed direction and tool axis direction.

## 5. CONCLUSIONS

Chatter avoidance often entails the adoption of conservative cutting parameters, reducing process performances. In some case this reduction is not admissible and cutting in chatter condition is preferred. However, the main drawback of adopting such an approach in finishing operations is the poor surface of the final product, characterized by a specific pattern, known as chatter marks. The generation of these marks was not yet deeply investigated, and specifically it was not clear how tool vibrations at high chatter frequency produce low frequency marks (i.e. wide marks) on the surface.

This paper presents an analysis of chatter marks generation mechanisms in milling, focusing on this issue, i.e. the spatial frequency contributions of the surface. The generation of the surface profile is regarded as a problem of sampling at the tooth pass frequency (in time domain) and reconstruction

(in spatial domain) of the cutting tool displacements. Using this analogy, two main effects (aliasing and pseudo moiré) causing chatter marks are highlighted, proposing specific analytical formulations to predict their spatial frequencies. The method was validated using reference surfaces generated by numerical models and experimental milled samples, confirming that the spectral proprieties of chatter marks are fundamentally defined by the two frequencies $sf_{c\text{-}a}$ and $sf_{pm}$ and their harmonics, as claimed in this work. Using the proposed formulations, the chatter marks spatial distribution can be predicted, given the values of spindle speed and chatter frequency. These parameters are critical and need to be accurately determined, especially for pseudo moiré effects identification.

Chatter frequency can be derived either by process simulation or experiments. In the first case, the computational efficiency and accuracy of the simulation are key aspects, however, chatter frequency can be identified analytically by simplified models or numerically simulating only a small portion of the cutting process. On the other hand, dedicated experimental approaches can provide the chatter frequency pattern over spindle speed (e.g., [28,29]) to be used to feed the proposed formulations.

Another issue to be considered is related to the periodicity of the process, assumed equal to the tooth pass frequency in this work (as in most of the works concerning chatter stability), that could change in case of high value of runout and significant uneven cutter pitch angles.

The prediction of chatter marks pattern could support the selection of cutting parameters, that enables the generation of an acceptable surface (e.g., small wavelengths marks, regular surface without visible defects) even in an unstable cutting condition.

This paper shows that in the singular conditions, in which chatter frequency is $k/h$ times the tooth pass frequency (where $k$ and $h$ integers), pseudo-moiré "beating" effects do not occur, leading to a regular surface pattern characterized by wavelengths multiple of the feed per tooth. This condition should be further analyzed along with an investigation on the chatter marks amplitude.

In addition, the paper contributes to the understanding of the chatter marks generation mechanism that could be useful for the development of effective chatter detection strategies and for the definition of corrective measures to ensure a better workpiece surface quality (e.g., toolpath compensation or active actuation of the workpiece as in [30,31]).

## REFERENCES


[1] P.G. Benardos, G.C. Vosniakos, Predicting surface roughness in machining: a review, Int. J. Mach. Tools Manuf. 43 (2003) 833–844. doi:10.1016/S0890-6955(03)00059-2.

[2] T.L. Schmitz, B.P. Mann, Closed-form solutions for surface location error in milling, Int. J. Mach. Tools Manuf. 46 (2006) 1369–1377. doi:http://dx.doi.org/10.1016/j.ijmachtools.2005.10.007.

[3] I. Marinescu, D.A. Axinte, An automated monitoring solution for avoiding an increased number of surface anomalies during milling of aerospace alloys, Int. J. Mach. Tools Manuf. 51 (2011) 349–357. doi:10.1016/j.ijmachtools.2010.10.005.

[4] P.G. Benardos, G.C. Vosniakos, Prediction of surface roughness in CNC face milling using neural networks and Taguchi's design of experiments, Robot. Comput. Integr. Manuf. 18 (2002) 343–354. doi:10.1016/S0736-5845(02)00005-4.

[5] T.L. Schmitz, J. Couey, E. Marsh, N. Mauntler, D. Hughes, Runout effects in milling: Surface finish, surface location error, and stability, Int. J. Mach. Tools Manuf. 47 (2007) 841–851. doi:10.1016/j.ijmachtools.2006.06.014.

[6] P. Dépincé, J.-Y. Hascoët, Active integration of tool deflection effects in end milling. Part 1. Prediction of milled surfaces, Int. J. Mach. Tools Manuf. 46 (2006) 937–944. doi:10.1016/j.ijmachtools.2005.08.005.

[7] K.A. Desai, P.V.M. Rao, On cutter deflection surface errors in peripheral milling, J. Mater. Process. Technol. 212 (2012) 2443–2454. doi:10.1016/j.jmatprotec.2012.07.003.

[8] Y. Altintas, Manufacturing Automation: Metal Cutting Mechanics, Machine Tool Vibrations, and CNC Design, (2012).

[9] K.S. Moon, J.W. Sutherland, The Origin and Interpretation of Spatial Frequencies in a Turned Surface Profile, J. Eng. Ind. 116 (1994) 340–347.

[10] Y. Liu, X. Wang, J. Lin, W. Zhao, Experimental investigation into the effect of chatter on surface micro-topography of gears in grinding, Proc. Inst. Mech. Eng. Part C J. Mech. Eng. Sci. 231 (2017) 294–308. doi:10.1177/0954406216642259.

[11] S.C. Lin, M.F. Chang, A study on the effects of vibrations on the surface finish using a surface topography simulation model for turning, Int. J. Mach. Tools Manuf. 38 (1998) 763–782. doi:10.1016/S0890-

6955(97)00073-4.
[12] E. Plaza, P. López, Surface roughness monitoring by singular spectrum analysis of vibration signals, Mech. Syst. Signal Process. 84 (2017) 516–530. doi:10.1016/j.ymssp.2016.06.039.
[13] S. Seguy, G. Dessein, L. Arnaud, Surface roughness variation of thin wall milling, related to modal interactions, Int. J. Mach. Tools Manuf. 48 (2008) 261–274. doi:10.1016/j.ijmachtools.2007.09.005.
[14] G. Peigne, H. Paris, D. Brissaud, A. Gouskov, Impact of the cutting dynamics of small radial immersion milling operations on machined surface roughness, Int. J. Mach. Tools Manuf. 44 (2004) 1133–1142. doi:10.1016/j.ijmachtools.2004.04.012.
[15] R. Shiota, T. Furuki, T. Hirogaki, E. Aoyama, Investigation of Control Methods of Chatter Vibration Based on Analysis of End-Milling Chatter Mark, Adv. Mater. Res. 1136 (2016) 639–644. doi:10.4028/www.scientific.net/AMR.1136.639.
[16] N. Lei, M. Soshi, Vision-based system for chatter identification and process optimization in high-speed milling, Int. J. Adv. Manuf. Technol. 89 (2017) 2757–2769. doi:10.1007/s00170-016-9770-2.
[17] G. Stepan, M. Toth, D. Bachrathy, S. Ganeriwala, M.S. Forum, Spectral Properties of Milling and Machined Surface, Mater. Sci. Forum. 836–837 (2016) 570–577. doi:10.4028/www.scientific.net/MSF.836-837.570.
[18] S. Kalpakjian, S.R. Schmid, Manufacturing Processes for Engineering Materials, Pearson Education, 2008.
[19] W.-S. Yun, J.H. Ko, D.-W. Cho, K.F. Ehmann, Development of a virtual machining system, part 2: prediction and analysis of a machined surface error, Int. J. Mach. Tools Manuf. 42 (2002) 1607–1615. doi:10.1016/S0890-6955(02)00138-4.
[20] C.E. Shannon, Communication in the Presence of Noise, Proc. IRE. 37 (1949) 10–21. doi:10.1109/JRPROC.1949.232969.
[21] I. Amidror, Sub-Nyquist artefacts and sampling moiré effects, R. Soc. Open Sci. 2:140550 (2015) 1–15. doi:10.1098/rsos.140550.
[22] A. Scippa, N. Grossi, G. Campatelli, Milled Surface Generation Model for Chip Thickness Detection in Peripheral Milling, Procedia CIRP. 8 (2013) 450–455. doi:http://dx.doi.org/10.1016/j.procir.2013.06.132.
[23] M.L. Campomanes, Y. Altintas, An Improved Time Domain Simulation for Dynamic Milling at Small Radial Immersions, J. Manuf. Sci. Eng. 125 (2003) 416–422. doi:10.1115/1.1580852.
[24] H. Paris, G. Peigne, R. Mayer, Surface shape prediction in high speed milling, Int. J. Mach. Tools Manuf. 44 (2004) 1567–1576. doi:10.1016/j.ijmachtools.2004.06.005.
[25] A. Scippa, F. Montevecchi, N. Grossi, L. Sallese, G. Campatelli, Time domain simulation model for active fixturing in milling, in: Proc. 8th Int. Conf. Lead. Edge Manuf. 21st Century, LEM 2015, Kyoto, Japan, 2015.
[26] L. Sallese, N. Grossi, A. Scippa, G. Campatelli, Numerical investigation of chatter suppression in milling using active fixtures in open-loop control, J. Vib. Control. 24 (2018) 1757–1773.
[27] L. Sallese, N. Grossi, A. Scippa, G. Campatelli, Investigation and correction of actual microphone response for chatter detection in milling operations, Meas. Control. 50 (2017) 45–52. doi:10.1177/0020294017702285.
[28] N. Grossi, A. Scippa, L. Sallese, R. Sato, Spindle speed ramp-up test: A novel experimental approach for chatter stability detection, Int. J. (2015).
[29] F. Ismail, E. Soliman, A new method for the identification of stability lobes in machining, Int. J. Mach. Tools Manuf. 37 (1997) 763–774. doi:http://dx.doi.org/10.1016/S0890-6955(96)00032-6.
[30] J.W. Sutherland, K.S. Moon, T.J. Stums, A.R. Kashani, Surface Texture Improvement in the Turning Process Via Application of a Magnetostrictively Actuated Tool Holder, 120 (2013) 193–199. doi:10.1115/1.2802409.
[31] L. Sallese, G. Innocenti, N. Grossi, A. Scippa, R. Flores, M. Basso, et al., Mitigation of chatter instabilities in milling using an active fixture with a novel control strategy, Int. J. Adv. Manuf. Technol. 89 (2017) 2771–2787. doi:10.1007/s00170-016-9831-6.

**On the generation of chatter marks in peripheral milling: a spectral interpretation**
N. Grossi, A. Scippa, L. Sallese, F. Montevecchi, G. Campatelli

**ACKNOWLEDGMENTS**
The authors would like to thank the DMG Mori Seiki Co. and the Machine Tool Technology Research Foundation (MTTRF) for the loaned machine tool (Mori Seiki NMV1500DCG 5-axes vertical-type machining centre).

HIGHLIGTHS

- An insight of the surface generation mechanism in milling is proposed
- Surface profile is regarded as a problem of sampling at the $f_{tp}$ of the tool vibrations
- Two fundamental spatial frequencies are identified, composing chatter marks surface
- Formulations to predict spectral proprieties of chatter marks are provided
- Numerical and experimental tests prove the accuracy of the proposed approach